Supplementary Information for:

A switchable green emitting dye and its phenomenal properties: implications for the photoluminescence features of carbon dots

Wiktor Kasprzyk*, Piotr P. Romańczyk*, Stefan S. Kurek* and Tomasz Świergosz†

Biotechnology and Physical Chemistry, Faculty of Chemical Engineering and Technology, Cracow University of Technology, ul. Warszawska 24, 31-155 Kraków, Poland

†Deceased in 2022.

E-mail: wiktor.kasprzyk@pk.edu.pl (WK); piotrom@pk.edu.pl (PPR); skurek@pk.edu.pl (SSK)

Table of contents

Additional Figures

Additional Tables

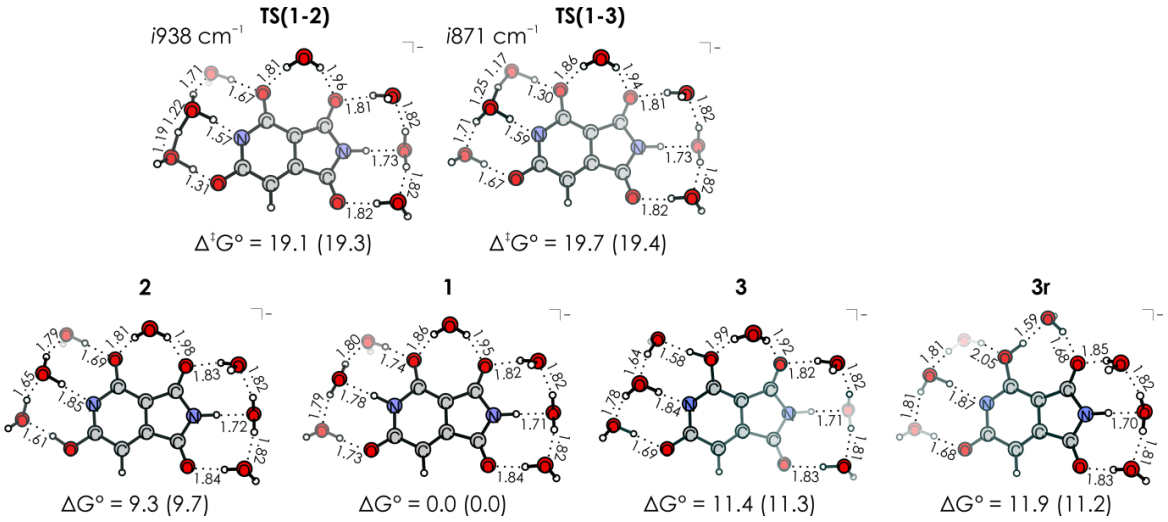

Figure S1. DFT-D-optimized ground-state geometries of $HPPT^{-}$ tautomers and transition states for proton transfer between them in aqueous medium; distances in Å. Given are relative Gibbs free energy differences (in kcal·mol^{-1}) computed at the DLPNO-CCSD(T)/*TightPNO*/CBS(T-Q) level with PCM (SMD) solvation. $\Delta G°$ values calculated at the SMD/B3LYP-D3/6-311++G(2d,2p) level are virtually the same as the values received from the high-level CC method (max. dev. 0.3 kcal·mol^{-1}), however, the barriers are underestimated by 2.5–2.7 kcal·mol^{-1}. The structures (not shown) with two protons in the five-membered ring, attached to the N atom and one of the O atoms, have energies near or above 30 kcal·mol^{-1}.

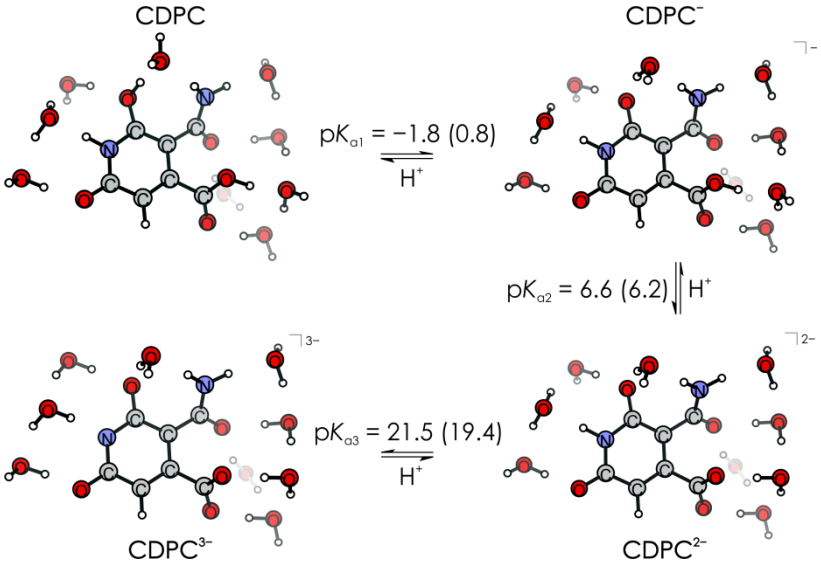

Figure S2. DFT-D-optimized ground-state geometries of CDPC acid-base forms used to calculate pK_as in water at the DLPNO-CCSD(T)/*TightPNO*/CBS(T-Q) level with PCM (SMD) solvation.

Table S1. pK_as of HPPT and CDPC acid-base forms in water, calculated at the DLPNO-CCSD(T)/TightPNO/CBS(T-Q) level for DFT-D structures shown in Figures 1 and S2 with the PCM (or SMD, in italics) solvation with or without microhydration

Acid/base forms	Microhydration + PCM	PCM only
$HPPT^+/HPPT$	−8.37 (*−4.01*)	−13.14 (*−6.95*)
$HPPT/HPPT^-$	−0.78 [a] (*1.18*)	0.29 (*0.59*)
DHP [b]/DHP^-	4.86 (*5.91*)	5.78 (*6.41*)
$CDPC/CDPC^-$	−1.81 (*0.80*)	−2.06 (*−1.42*)
$CDPC^-/CDPC^{2-}$	6.59 (*6.16*)	12.42 (*8.24*)
$CDPC^{2-}/CDPC^{3-}$	21.49 (*19.39*)	31.16 (*24.99*)

[a]The *pseudo*-pK_a value of HPPT calculated from the changes observed in the spectra of $HPPT{\cdot}NH_4$ in 18% and 45% H_2SO_4, of Hammett acidity −0.9 and −2.9, respectively, is −0.94 (see Figure 2 in the main text). [b]2,6-Dihydroxypyridine, for which the measured pK_a value is 4.52.[1]

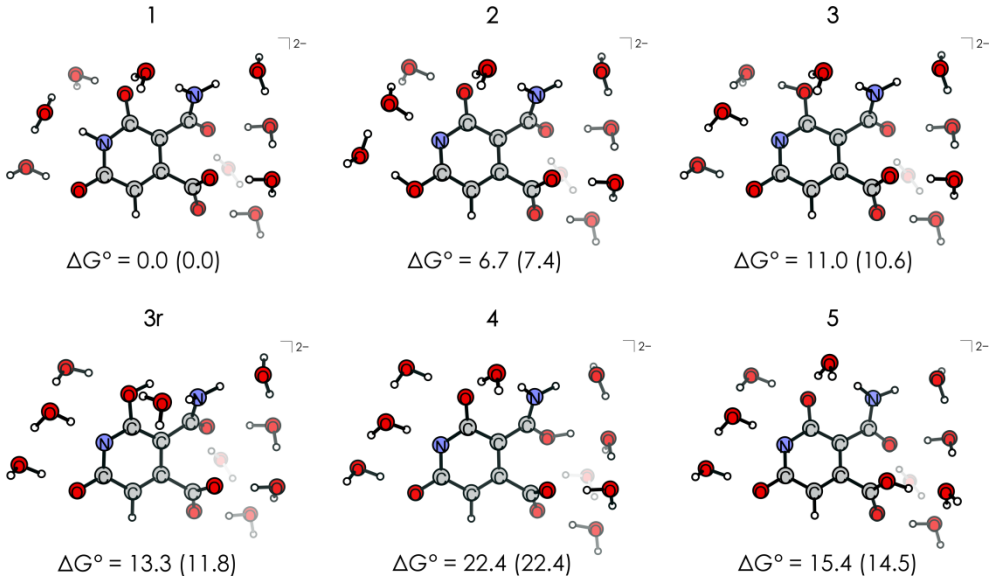

Figure S3. DFT-D-optimized ground-state geometries of $CDPC^{2-}$ tautomers in aqueous medium. Given are relative Gibbs free energy differences (in kcal·mol^{-1}) computed at the DLPNO-CCSD(T)/*TightPNO*/CBS(T-Q) level with PCM (SMD) solvation.

(1) E. Spinner, J. C. B. White, Spectral and ionisation constant studies of substituted 2-hydroxypyridines (1,2-dihydro-2-oxopyridines), *J. Chem. Soc. B*, **1966**, 991–995, DOI: 10.1039/J29660000991.

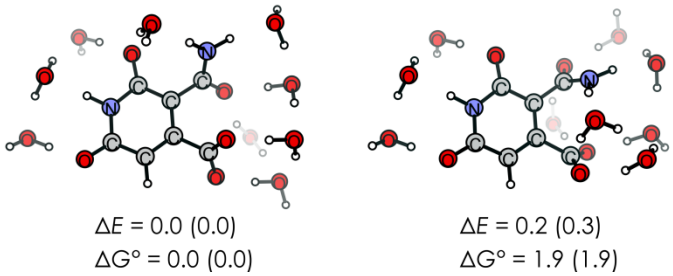

Figure S4. DFT-D-optimized ground-state geometries of $CDPC^{2-}$ rotamers in aqueous medium; distances in Å. Given are relative electronic energy and Gibbs free energy differences (in kcal·mol^{-1}) computed at the DLPNO-CCSD(T)/*TightPNO*/CBS(T-Q) level with PCM (SMD) solvation.

Gibbs binding energy of $HPPT^-$ and NH_4^+

The Gibbs binding energy ($\Delta_{bind}G°$) of $HPPT^-$ and NH_4^+ ions was evaluated in aqueous solution. At first sight, two oxygen atoms in the structure of $HPPT^-$, displaying most negative electrostatic potential (see Figure S5), form a bidentate site, which is ideally suited to bind NH_4^+ via two H-bonds. However, the formation of such an adduct was found to be disfavored in aqueous solution. An optimization of $HPPT{\cdot}NH_4$ microsolvated by nine explicit water molecules (three additional waters are needed to ensure appropriate solvation of NH_4^+) leads to a structure where NH_4^+ interacts with $HPPT^-$ via only one moderate N–H···O hydrogen bonding as shown in Figure S6. Positive or slightly negative $\Delta_{bind}G°$ values (depending on solvation model) computed for this adduct are in line with the experiment revealing dissociation of $HPPT{\cdot}NH_4$ occurring at concentrations much lower than the standard-state.

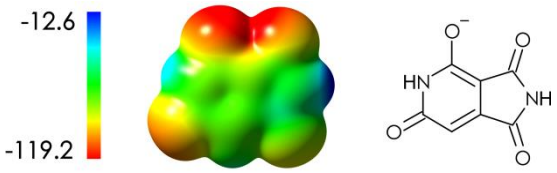

Figure S5. Molecular electrostatic potential map (kcal·mol^{-1}) on the 0.001 a.u. isosurface of $HPPT^-$ electronic density obtained at the SMD/B3LYP/6-311++G(2d,2p) level.

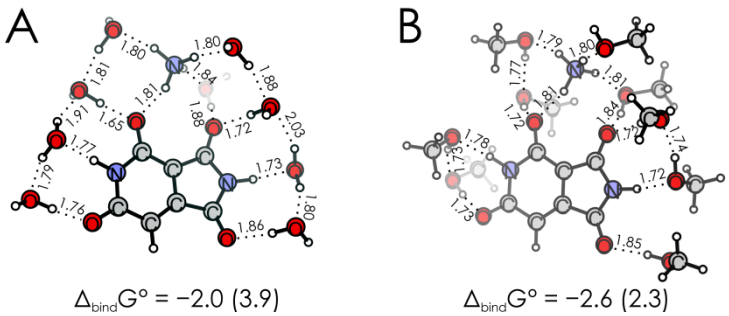

Figure S6. DFT-D-optimized ground-state geometries of $HPPT^-{\cdot}NH_4^+$ ion pairs in water (A) and methanol (B); distances in Å. Given are Gibbs free energies (in kcal·mol^{-1}) of NH_4^+ binding to $HPPT^-$ was calculated at the DLPNO-CCSD(T)/*TightPNO*/CBS(T-Q) level with PCM (SMD) solvation. $\Delta_{bind}G°$ values calculated at the SMD/B3LYP-D3/6-311++G(2d,2p) level with BSSE-correction are 0.3 (in water) or 1.2 (in methanol) kcal·mol^{-1} higher in comparison to the high-level CC method.

Electrochemical measurements

Voltammograms were registered at the scan rate of 0.1 V s^{-1} in phosphate buffers of pH 7 and 4.4 under 99.999% argon (Messer) atmosphere using a BAS 100B/W workstation. A glassy carbon type K disk (2.3 mm^2, Mineral, Poland) was used as the working electrode, platinum tape as the auxiliary and Ag/AgCl (3 M NaCl) as the reference. The most reliable potentials of redox processes were read from voltammogram semiderivatives. Semiderivatives are the derivatives of semiintegrals. These, in turn, show directly the changes in the concentration of the reactant at the electrode surface. At the inflection point of the semiintegral, concentrations of the reactant and the product of the electrode reactions are equal, and at this point the semiderivative shows a peak. The position of this peak for fast electrochemical processes, even if they are chemically irreversible (with no corresponding wave on the return scan), is thus equal to the formal potential. For processes with slow electron transfer a laborious and tedious convolution technique could be used.[1]

Cyclic voltammograms of HPPT·NH_4 recorded in phosphate buffers (Figure S7) show a distinct, pH-dependent reduction wave, at −1.12 and −0.93 V vs. Ag/AgCl at pH 7 and 4.4, respectively, and two oxidation waves, much less pH-dependent, at potentials equal to or more positive than 0.85 V. The observed processes are chemically irreversible, it is thus not possible to calculate $E_{1/2}$ corresponding to the formal potential, E_f (at which the concentrations of the oxidized and reduced forms are equal), and related to the standard potential of the electrode reaction. The peak potentials read from semiderivatives of voltammograms: −1.09 V and −0.91 V (reduction), and 0.86 V and 0.89 V (oxidation) at pH 7 and 4.4, respectively, are equal to formal potentials.

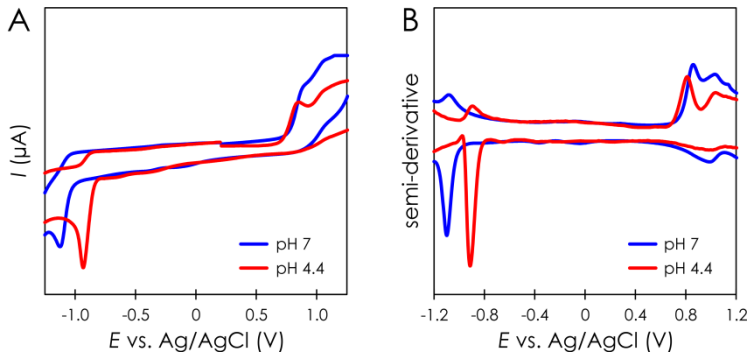

Figure S7. Cyclic voltammograms (A) and their semi-derivatives (B) for HPPT·NH_4 recorded at GCE in phosphate buffers of pH 7 and 4.4 (v = 0.1 V s^{-1}).

Calculation of pK_a from experimental spectra

The pK_a values were calculated from the Henderson-Hasselbalch equation. Where possible, the spectra of the pure forms were taken from the solutions, where the spectra did not change over a wide pH range. The value for the first dissociation of HPPT was based on the spectra of this compound in sulfuric acid. However, the result is approximate as we used Hammett acidity functions[2] instead of pH, so it should be treated as a *pseudo*-pK_a rather. In this case, in more concentrated sulfuric acid the changes in spectrum were more complex, so the spectrum of a pure form was obtained by subtracting a small portion of the spectrum in neutral solutions from a couple of spectra resulting in a reasonable spectrum and very close pK_a values. The ratios [A^-]/[HA] were determined from least-square fitting a

linear combination of the spectra of pure species to a spectrum at a given pH. The *pseudo*-pK_a thus calculated was equal to −0.94.

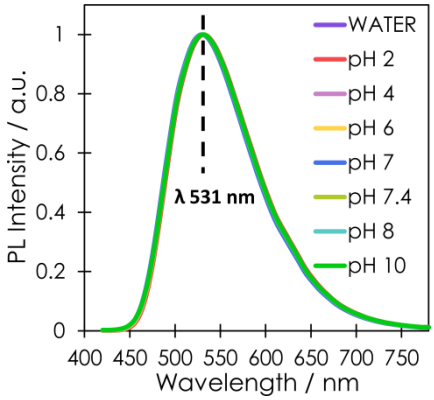

Figure S8. Normalised PL emission spectra of $HPPT^-$ solution in the pH range 2–10.

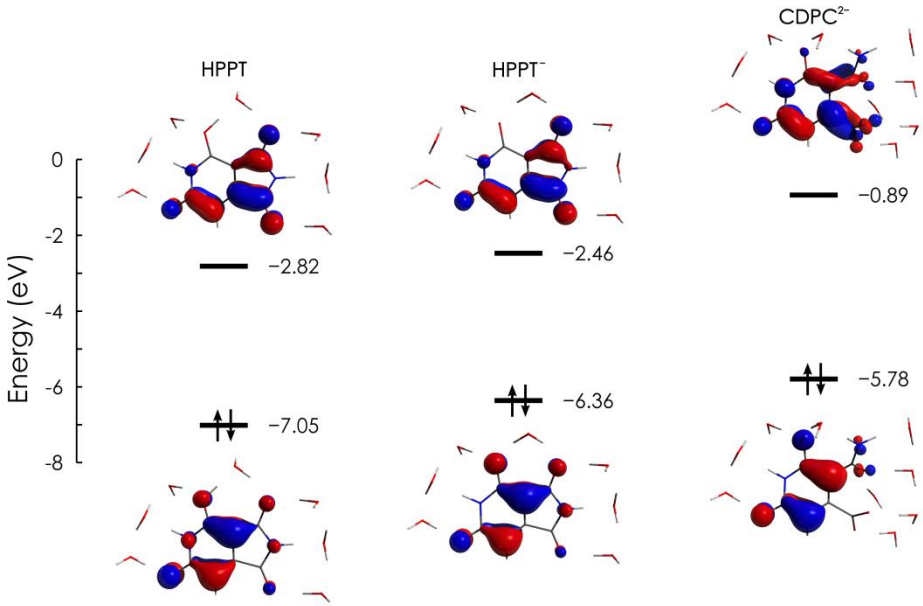

Figure S9. HOMO and LUMO contour plots (isovalue of 0.05 $bohr^{-3/2}$) and orbital energies computed for microhydrated HPPT, $HPPT^-$ and $CDPC^{2-}$ at the PCM/PBE0/6-311++G(2d,2p) level.

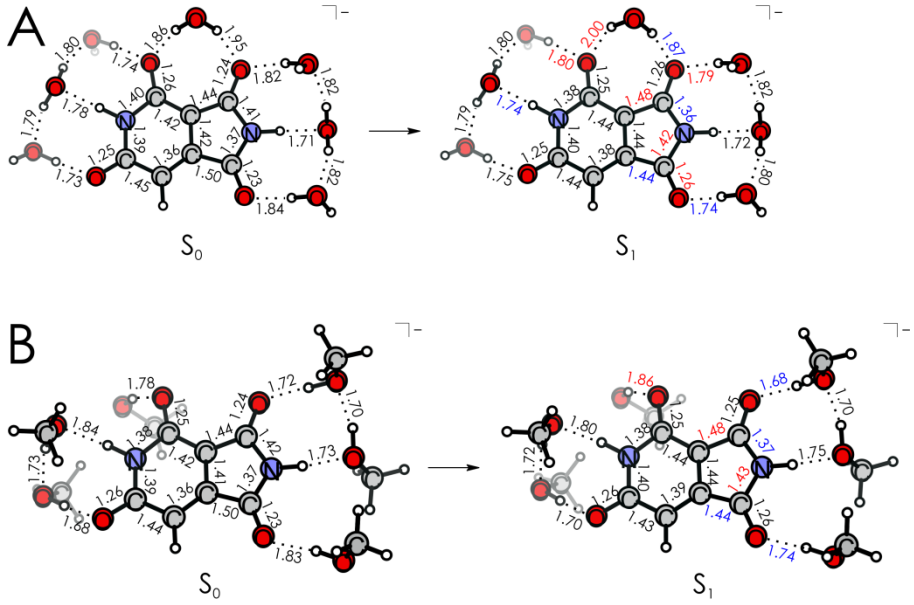

Figure S10. (TD)DFT-D-optimized ground-state and excited-state geometries of $HPPT^-$ microsolvated by (A) water and (B) methanol. Distances in Å; red color denotes increase (by 0.03 Å or more), and blue decrease (by 0.03 Å or more) upon excitation.

Table S2. Calculated vertical S_0–S_1 excitation (LR-PCM) and emission (SS-PCM) energies and oscillator strengths obtained at the PCM/TD-PBE0/6-311++G(2d,2p) level for structures with or without microhydration

Species (solvent) [a]	absorption / eV (nm)				emission / eV (nm)			
	PBE0		B3LYP		PBE0		B3LYP	
	ΔE (λ)	f	ΔE (λ)	f	ΔE (λ)	f	ΔE (λ)	f
$HPPT\cdots(H_2O)_7$	3.47 (357)	0.20	3.38 (367)	0.19	_ [b,c]	_ [b,c]	_ [b,c]	_ [b,c]
HPPT (water)	3.55 (349)	0.17	3.46 (358)	0.16	_ [b,c]	_ [b,c]	_ [b,c]	_ [b,c]
$HPPT\cdots(MeOH)_7$	3.46 (359)	0.20	3.37 (368)	0.19	_ [b]	_ [b]	_ [b]	_ [b]
HPPT (methanol)	3.56 (349)	0.17	3.46 (358)	0.16	_ [b]	_ [b]	_ [b]	_ [b]
$HPPT^-\cdots(H_2O)_6$	3.09 (402)	0.18	3.00 (413)	0.17	2.28 (544)	0.08	2.19 (565)	0.08
$HPPT^-\cdots(H_2O)_7$	3.13 (396)	0.19	3.05 (407)	0.18	2.30 (538)	0.09	2.22 (558)	0.08
$HPPT^-$ (water)	3.13 (396)	0.17	3.05 (407)	0.17	2.35 (527)	0.08	2.27 (546)	0.08
$HPPT^-NH_4^+\cdots(H_2O)_9$	3.11 (398)	0.19	3.03 (410)	0.18	_ [b]	_ [b]	_ [b]	_ [b]
$HPPT^-\cdots(MeOH)_6$	3.09 (401)	0.18	3.00 (413)	0.17	2.31 (536)	0.09	2.23 (555)	0.08
$HPPT^-\cdots(MeOH)_7$	3.13 (396)	0.18	3.05 (407)	0.17	2.29 (542)	0.09	2.21 (561)	0.08
$HPPT^-$ (methanol)	3.13 (396)	0.17	3.05 (407)	0.16	2.36 (526)	0.08	2.27 (546)	0.08
$HPPT^-NH_4^+\cdots(MeOH)_9$	3.13 (397)	0.19	3.04 (408)	0.18	_ [b]	_ [b]	_ [b]	_ [b]
$CDPC\cdots(H_2O)_9$	4.01 (309)	0.14	3.90 (318)	0.13	_ [b]	_ [b]	_ [b]	_ [b]
$CDPC^-\cdots(H_2O)_9$	3.78 (328)	0.21	3.68 (337)	0.19	_ [b]	_ [b]	_ [b]	_ [b]
$CDPC^-$ (water)	4.03 (308)	0.31	3.95 (314)	0.29	_ [b]	_ [b]	_ [b]	_ [b]
$CDPC^{2-}\cdots(H_2O)_9$	4.05 (306)	0.25	3.96 (313)	0.24	_ [b,c]	_ [b,c]	_ [b,c]	_ [b,c]
$CDPC^{2-}\cdots(H_2O)_9$ rotamer2	3.87 (320)	0.22	3.78 (328)	0.20	_ [b,c]	_ [b,c]	_ [b,c]	_ [b,c]
$CDPC^{2-}$ (water)	4.22 (294)	0.37	4.14 (300)	0.36	_ [b,c]	_ [b,c]	_ [b,c]	_ [b,c]
$CDPC^{3-}\cdots(H_2O)_9$	4.00 (310)	0.27	3.90 (318)	0.25	_ [b]	_ [b]	_ [b]	_ [b]

[a] In the case of microsolvated molecules, they are immersed in the continuum of the same solvent. [b] Not calculated. [c] Measured fluorescence too weak.

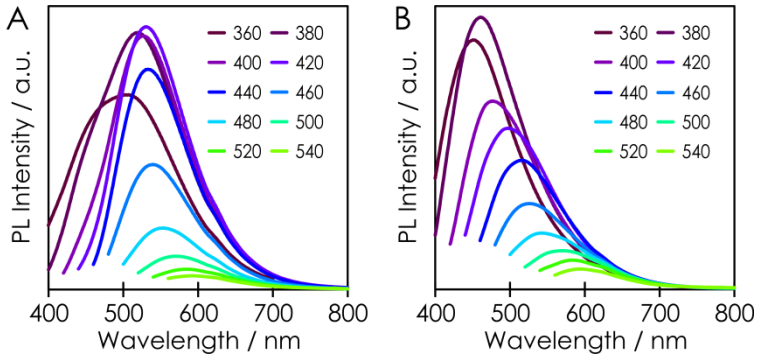

Figure S11. (A) Excitation-dependent PL emission of HPPT@CDs in aqueous solution (pH ~6), and (B) HPPT@CDs treated with 1 M NaOH for 60 min (pH of solution was adjusted to pH ~6 just prior to measurements). Numbers indicate excitation wavelengths in nm.

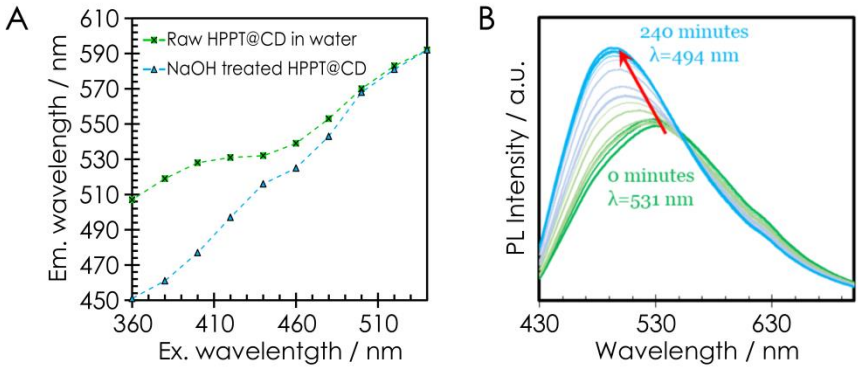

Figure S12. (A) PL emission maximum wavelengths plotted against respective excitation wavelengths; green marks and dashed line represent aqueous solution of raw CDs at pH ~6, blue marks and dashed line stand for aqueous solution of CDs treated with 1 M NaOH for 60 min (pH of solution was adjusted to pH ~6 just prior to optical measurements). (B) Changes in emission spectra (at 400 nm excitation wavelength) of HPPT@CDs CDs upon the progress of hydrolysis in 1 M NaOH.

LC-MS analyses and HPLC separation

LCMS-8030 (Shimadzu, Kyoto, Japan) mass spectrometric system coupled to an LC-20ADXR pump utilizing the LC gradient was used for analytical low-resolution LC-ESI-MS/MS analyses. The LC analyses were carried out on a 100 mm × 4.6 mm × 5.0 µm Kinetex C18 chromatographic column (Phenomenex, Torrance, CA, USA). Kinetex C18 chromatographic column was preceded by a guard column of the same material (Phenomenex, Torrance, CA, USA). The positive and negative ion chromatograms as well as mass spectra were acquired (electrospray voltage 4.5 kV; capillary temperature 250 °C), and controlled via LabSolutions software version 5.91 (Shimadzu, Kyoto, Japan). The MS unit was preceded by DAD detector (SPD-M20A, Shimadzu) in the analytical system. The DAD detector acquired absorption spectra in the 190-800 nm range. The injection volume was 5 µL, and the flow rate was 1 mL/min. The column was thermostated at 40 °C. The separation of the analytes was performed with binary gradient elution. The mobile phases were: A − 2% formic acid in demineralized water, and B − pure methanol. The gradient profile was: (t [min], % B), (0, 0.1), (7, 0.1), (13, 30), (13.01, 90), (14, 90).

Preparative HPLC system with LC-20AP pumps, UV-Vis SPD-20AV detector and LabSolutions 5.51 operating software was used (Shimadzu Corp., Japan) equipped with a preparative column C18 (250 mm × 50 mm i.d., 30 µm) (Interchim, France) with a 30 mm x 10 mm i.d. guard column of the same material under the following gradient system: (t[min], % A, % B, % C), (0, 100, 0, 0), (10, 100, 0, 0), (50, 0, 10, 90), (60, 0, 70, 30), (62, 0, 70, 30). The mobile phases were: A − demineralized water, B − pure acetone, C − 0.1% formic acid in water. The injection volume was 30 mL and the flow rate was 50 mL/min. Detection was performed at 350 and 254 nm with a PDA UV –Vis detector; column temp. 30 °C. Purity of the products was confirmed using LC-DAD-MS.

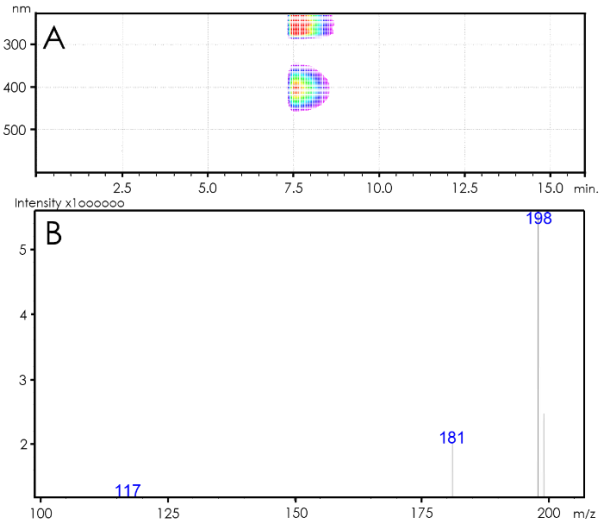

Figure S13. LC-DAD chromatogram of (A) purified HPPT and (B) ESI-MS spectrum showing peak with m/z 198 corresponding to HPPT ammonium salt.

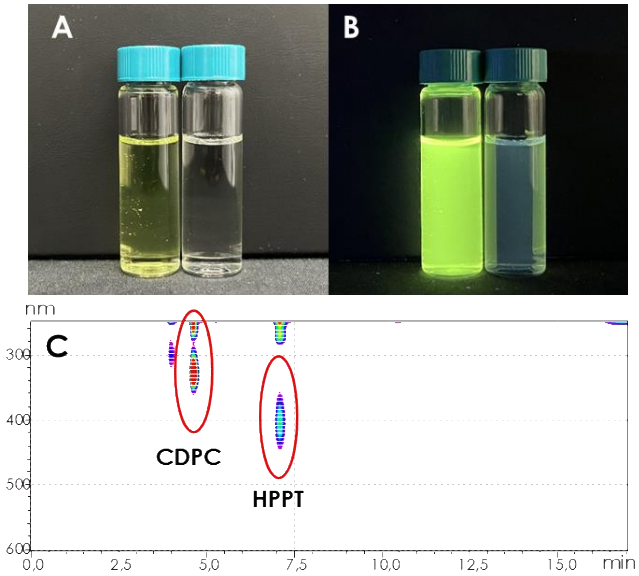

Figure S14. Photos of 3-carbamoyl-2,6-dihydroxypyridine-4-carboxylic acid (right vial) in neutral and (left vial) in HCl acidified aqueous solutions under (A) daylight and (B) UV irradiation (365 nm), and (C) LC-DAD chromatogram of the acidified sample.

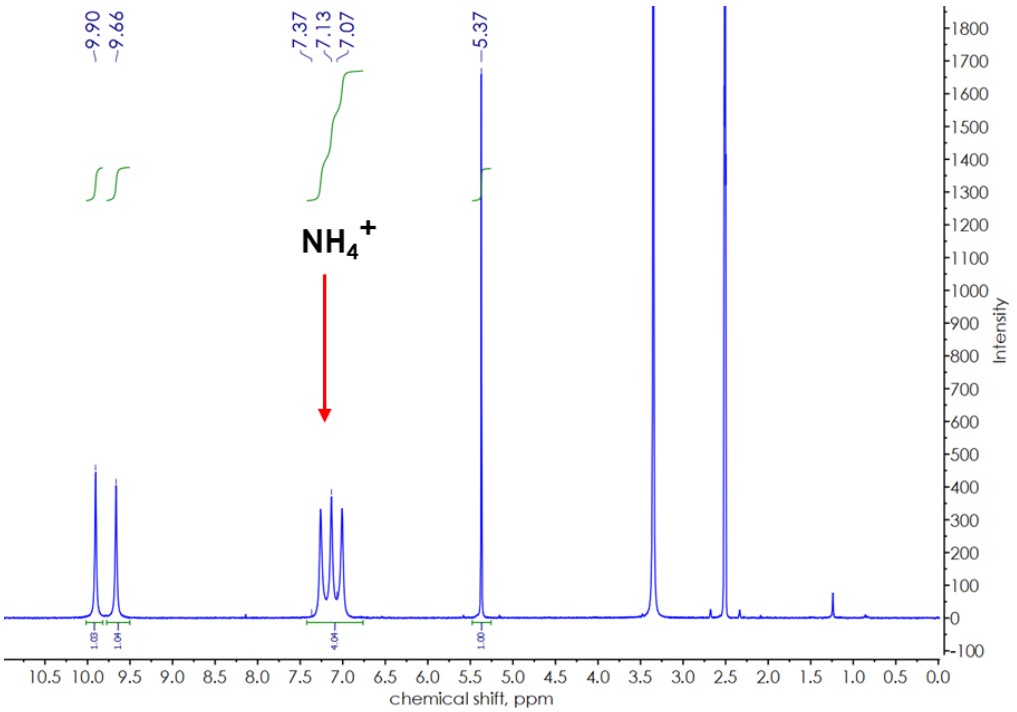

Figure S15. ^{1}H NMR spectrum of HPPT ammonium salt in DMSO-d_6. The NH_4^+ triplet is observed at ca. 7.1 ppm, $^{1}J_{1H-14N}$ = 52 Hz; the signals at ca. 2.5 ppm and 3.3 ppm are due to DMSO and H_2O, respectively.

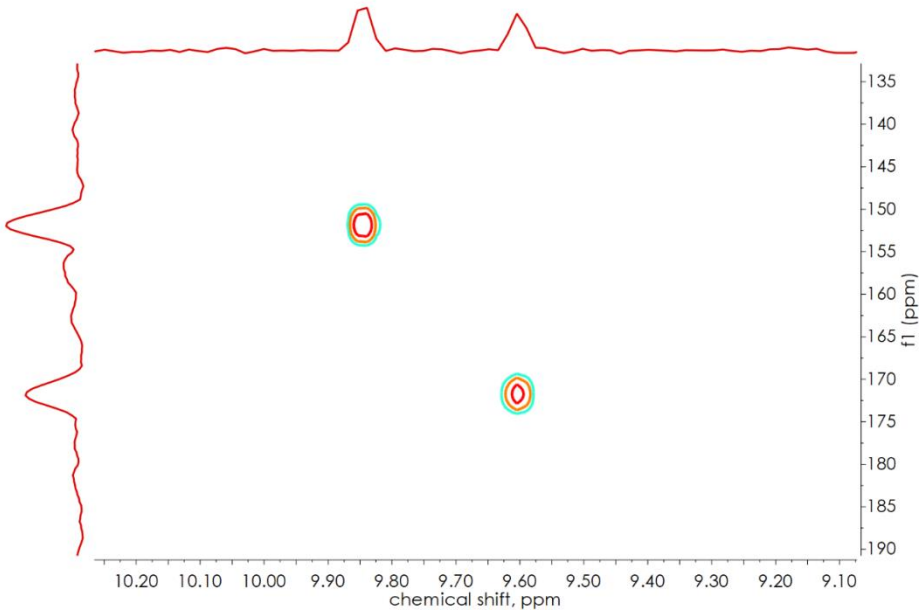

Figure S16. ^{15}N-^{1}H HMQC NMR spectrum of HPPT ammonium salt in DMSO-d_6.

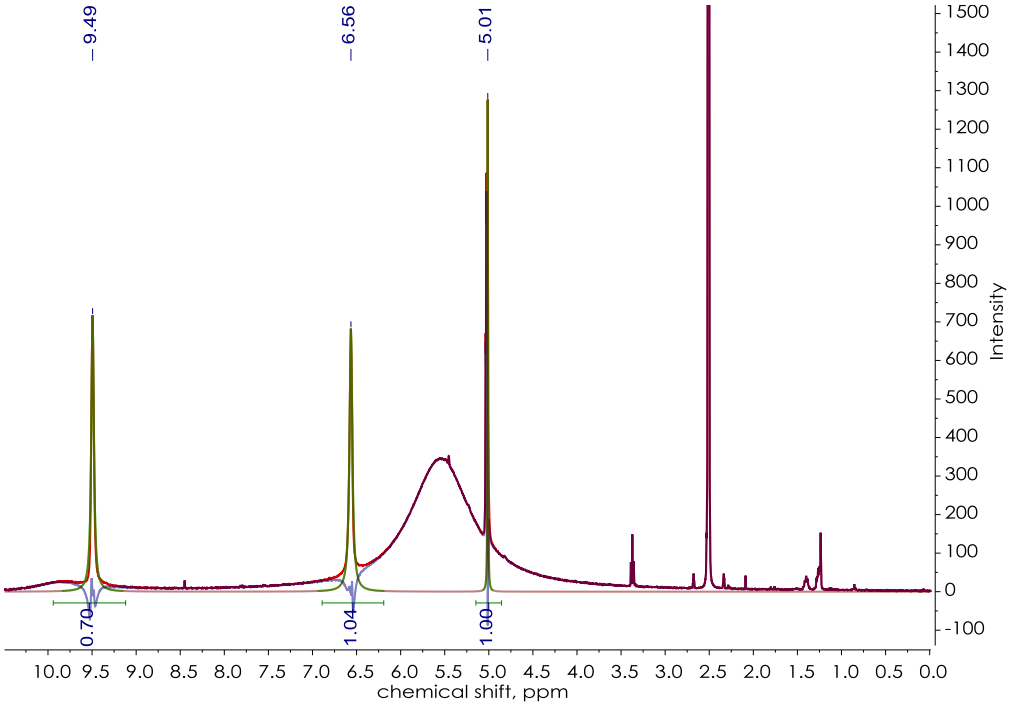

Figure S17. ^{1}H NMR spectrum of 3-carbamoyl-2,6-dihydroxypyridine-4-carboxylic acid (CDPC) in DMSO-d_6.

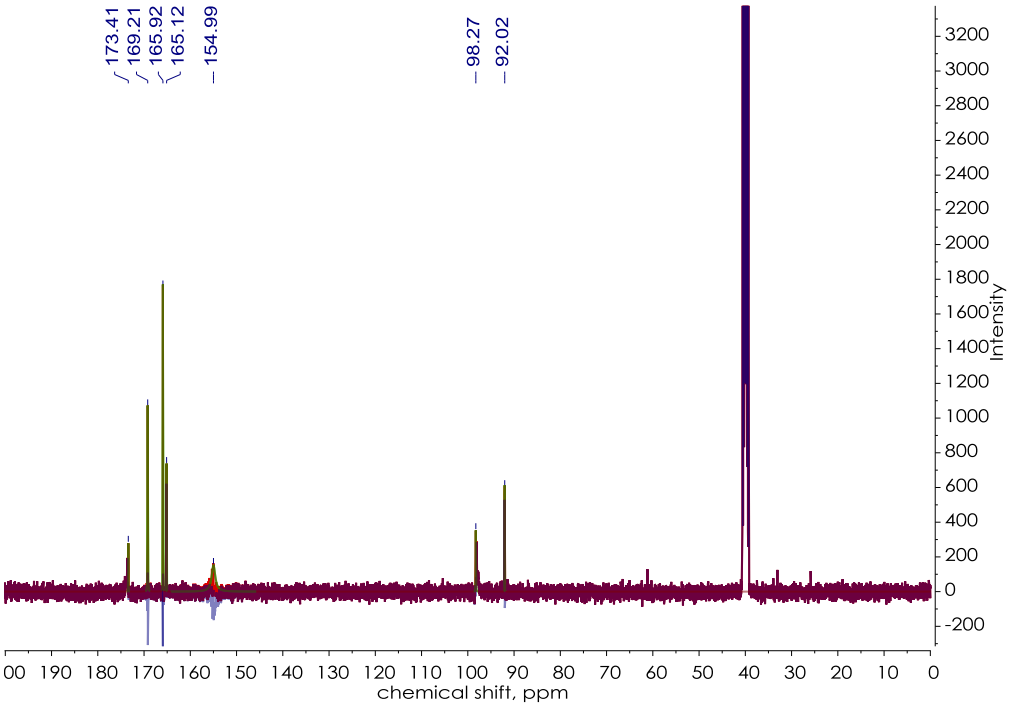

Figure S18. ^{13}C NMR spectrum of 3-carbamoyl-2,6-dihydroxypyridine-4-carboxylic acid (CDPC) in DMSO-d_6.

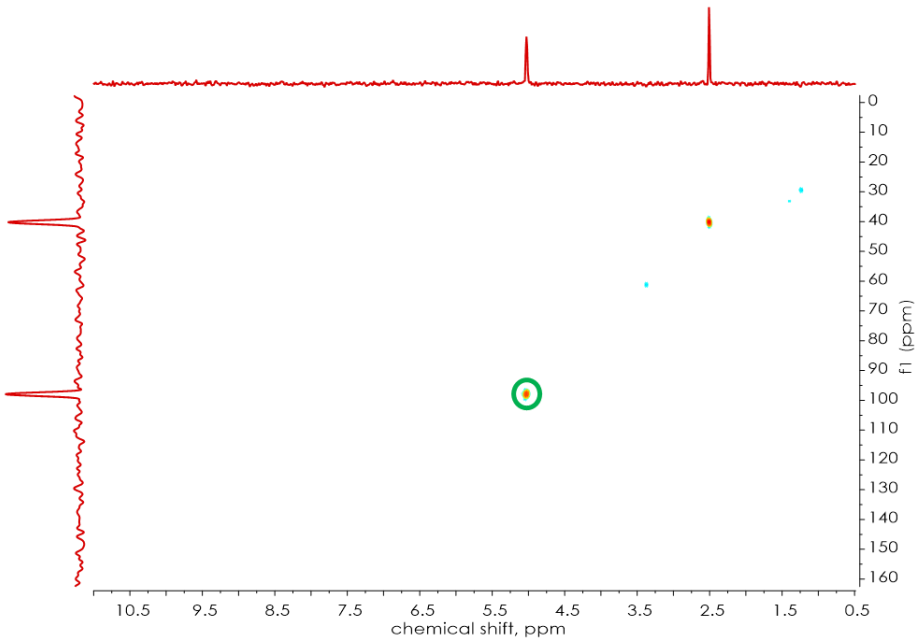

Figure S19. ^{1}H-^{1}H COSY NMR spectrum of 3-carbamoyl-2,6-dihydroxypyridine-4-carboxylic acid (CDPC) in DMSO-d_6.

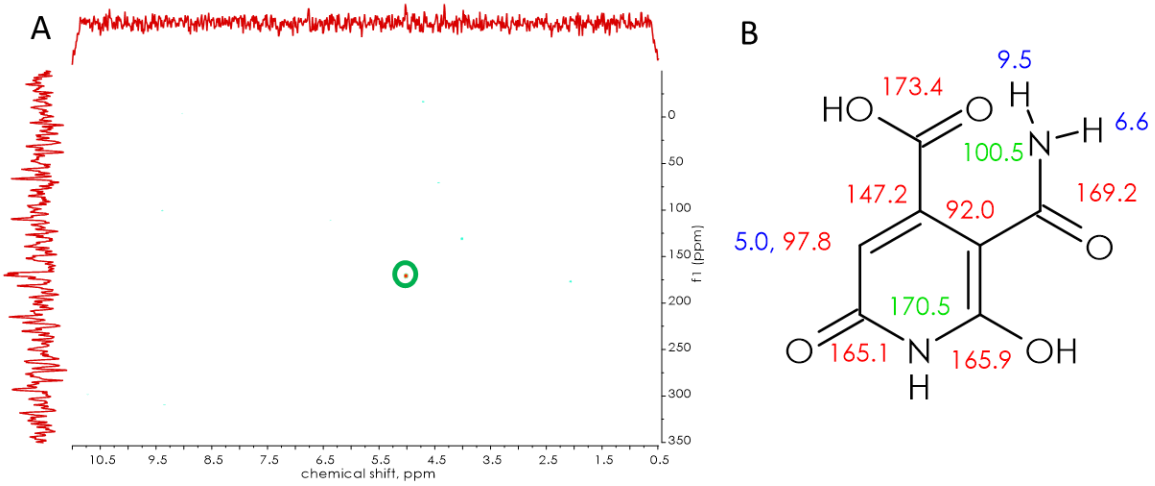

Figure S20. (A) ^{15}N-^{1}H HMBC NMR spectrum of 3-carbamoyl-2,6-dihydroxypyridine-4-carboxylic acid (CDPC) in DMSO-d_6 and (B) chemical structure of CDPC with NMR assignments (ppm).

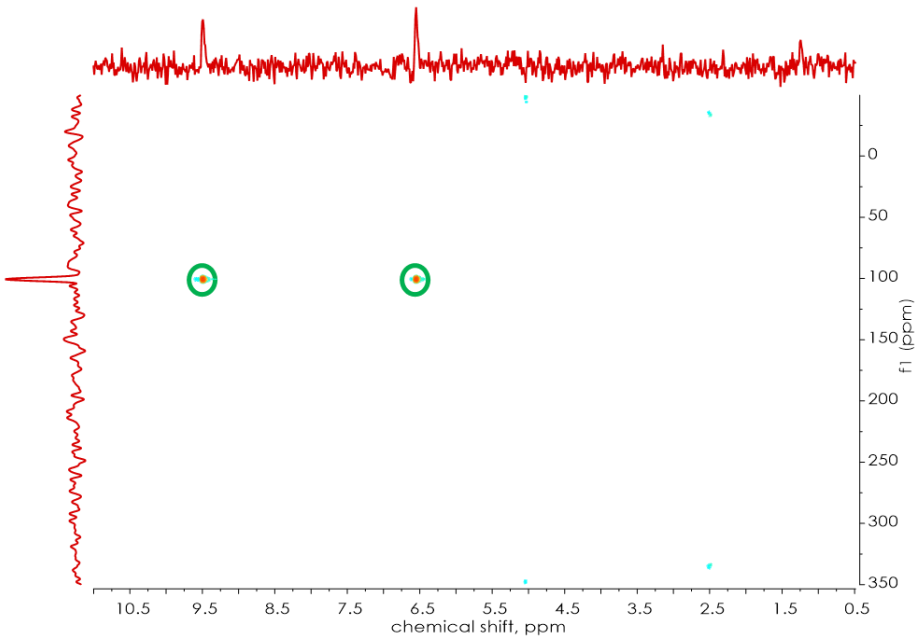

Figure S21. ^{13}C-^{1}H HMBC NMR spectrum of 3-carbamoyl-2,6-dihydroxypyridine-4-carboxylic acid (CDPC) in DMSO-d_6.

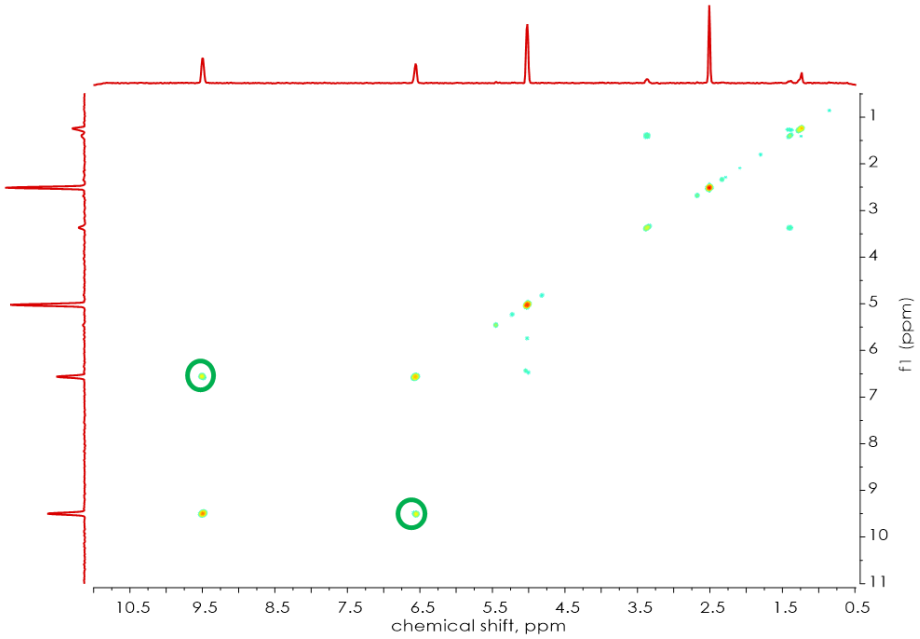

Figure S22. ^{13}C-^{1}H HSQC NMR spectrum of 3-carbamoyl-2,6-dihydroxypyridine-4-carboxylic acid (CDPC) in DMSO-d_6.

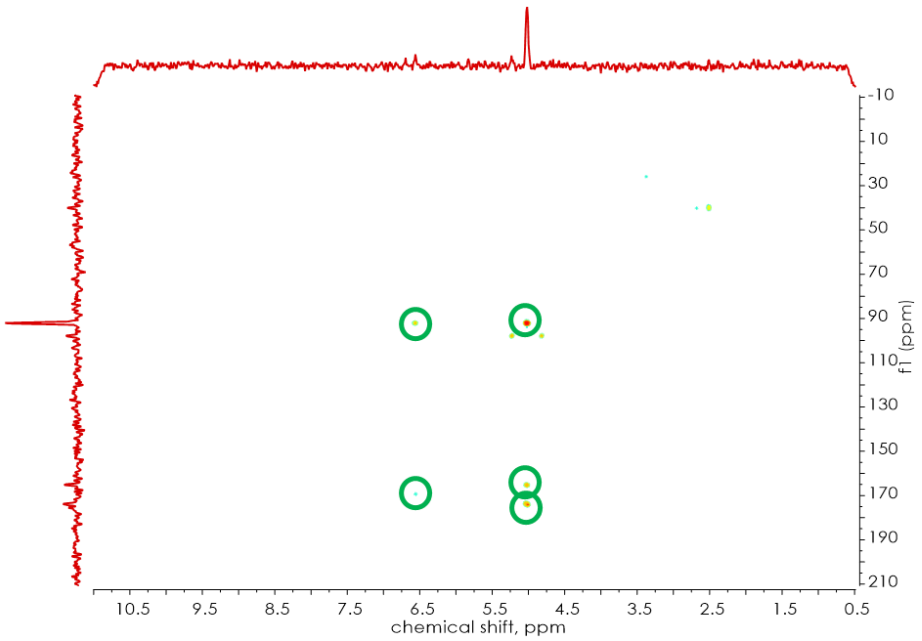

Figure S23. ^{15}N-^{1}H HSQC NMR spectrum of 3-carbamoyl-2,6-dihydroxypyridine-4-carboxylic acid (CDPC) in DMSO-d_6.

Additional references

1 P. P. Romańczyk, G. Rotko and S. S. Kurek, Dissociative electron transfer in polychlorinated aromatics. Reduction potentials from convolution analysis and quantum chemical calculations, *Phys. Chem. Chem. Phys.*, 2016, **18**, 22573–22582. DOI: 10.1039/c6cp02222g

2 C. D. Johnson, A. R. Katritzky and S. A. Shapiro, Temperature Variation of the H_0 Acidity Function in Aqueous Sulfuric Acid Solution, *J. Am. Chem. Soc.*, 1969, **91**, 6654–6662. DOI: 10.1021/ja01052a021

Complete reference 30 (in the main text):

30 M. J. Frisch, G. W. Trucks, H. B. Schlegel, G. E. Scuseria, M. A. Robb, J. R. Cheeseman, G. Scalmani, V. Barone, B. Mennucci, G. A. Petersson, H. Nakatsuji, M. Caricato, X. Li, H. P. Hratchian, A. F. Izmaylov, J. Bloino, G. Zheng, J. L. Sonnenberg, M. Hada, M. Ehara, K. Toyota, R. Fukuda, J. Hasegawa, M. Ishida, T. Nakajima, Y. Honda, O. Kitao, H. Nakai, T. Vreven, J. A. Montgomery Jr., J. E. Peralta, F. Ogliaro, M. Bearpark, J. J. Heyd, E. Brothers, K. N. Kudin, V. N. Staroverov, T. Keith, R. Kobayashi, J. Normand, K. Raghavachari, A. Rendell, J. C. Burant, S. S. Iyengar, J. Tomasi, M. Cossi, N. Rega, J. M. Millam, M. Klene, J. E. Knox, J. B. Cross, V. Bakken, C. Adamo, J. Jaramillo, R. Gomperts, R. E. Stratmann, O. Yazyev, A. J. Austin, R. Cammi, C. Pomelli, J. W. Ochterski, R. L. Martin, K. Morokuma, V. G. Zakrzewski, G. A. Voth, P. Salvador, J. J. Dannenberg, S. Dapprich, A. D. Daniels, O. Farkas, J. B. Foresman, J. V. Ortiz, J. Cioslowski and D. J. Fox, *Gaussian 09, Revision E.01*, Gaussian, Inc., Wallingford, CT, 2013.